
DNS Study of spatial discrete suction for Laminar Flow Control

Ralf Messing and Markus Kloker

Institut für Aerodynamik und Gasdynamik, Universität Stuttgart, Pfaffenwaldring
21, 70550 Stuttgart, Germany, e-mail: [last name]@iag.uni-stuttgart.de

By means of spatial direct numerical simulations (DNS) based on the complete Navier-Stokes equations the effect of three-dimensional discrete suction on the spatial development of a laminar boundary-layer flow generic for the front part of a swept-back airliner wing has been investigated. The baseflow is an accelerated Falkner-Skan-Cooke boundary layer, on a swept wedge with semi-opening angle of 45° (Hartree parameter $\beta_H = 0.5$) which is mainly characterised by crossflow instability. The simulations of the microscale phenomena confirm that 3-d suction at the wall can excite unstable crossflow disturbances that have to be minimised by using either slot arrays or hole arrays with high porosity, otherwise the stabilising (2-d) effect of suction is compromised. Premature transition through oversuction could be identified as a convective secondary instability of the flow field deformed by strong steady crossflow vortices emerging from the suction panel.

1 Introduction

For the next two decades a doubling of world-wide air traffic accompanied by a simultaneous shortage of crude oil reserves is predicted. Therefore it will become mandatory to palpably reduce the specific fuel consumption of aircrafts for environmental and economic reasons. As fuel consumption during cruise is mainly determined by viscous drag its reduction offers the greatest potential for fuel savings. The concept of hybrid laminar flow control (HLFC) on the wing consists of a combination of surface suction, applied in the upper front part, and of a designed extended region of favourable pressure gradient, attained by profile shaping. This technology has shown its capability in significantly delaying laminar-turbulent transition in recent flight experiments in the United States [4, 5] and Europe [2, 7]. European efforts culminated in an extensive flight program on an A320 with modified vertical fin enabling also suction in the nose region. Laminar flow could be maintained up to 50% chord

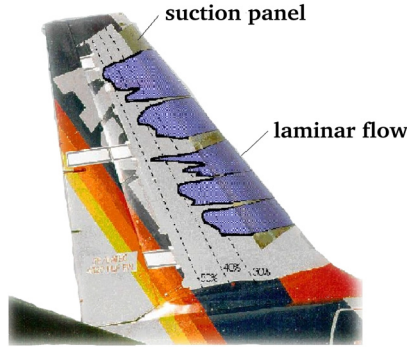


Fig. 1. Vertical Fin of the A320 Fin Experiment. The suction panel extends to 20% chord. The blue area indicates laminar flow.

at a flight Mach number $Ma = 0.82$. All recent flight experiments used panels perforated by laser-drilled microholes to suck air off the boundary-layer. The holes are typically 50 – 100 microns in diameter, the hole spacing lies between 500 – 800 microns leading to a porosity of the panel of 0.5 – 1%. In the early days of suction-flight experiments spanwise stripes were used due to the inability to manufacture micro-holes [3, 6]. As we will see this perforation geometry has advantages from the hydrodynamics stability point of view.

As a direct consequence of a spanwise inhomogeneous suction distribution stationary 3-d disturbances are generated which can be amplified in a three-dimensional boundary layer according to prediction by linear stability theory. Eigenmodal growth of these disturbances constitutes the major difference to two-dimensional boundary layers without crossflow where stationary modes are typically damped. (In respective DNS we never observed relevant so-called algebraic transient growth.) For illustration simulations have been performed for a single spanwise row of suction holes on an unswept and a swept wedge (Fig. 2). In case of the unswept wedge a pair of counterrotating vortices is generated at each suction hole. They quickly decay downstream of the hole row. In the swept case again a pair of counterrotating vortices emerges at each hole. The counterclockwise rotating vortex that would transport fluid against the basic crossflow close to the wall is suppressed rapidly whereas the clockwise rotating vortex grows continuously downstream.

2 Numerical Method

The governing equations are the full 3-d incompressible unsteady Navier-Stokes equations in vorticity-velocity formulation :

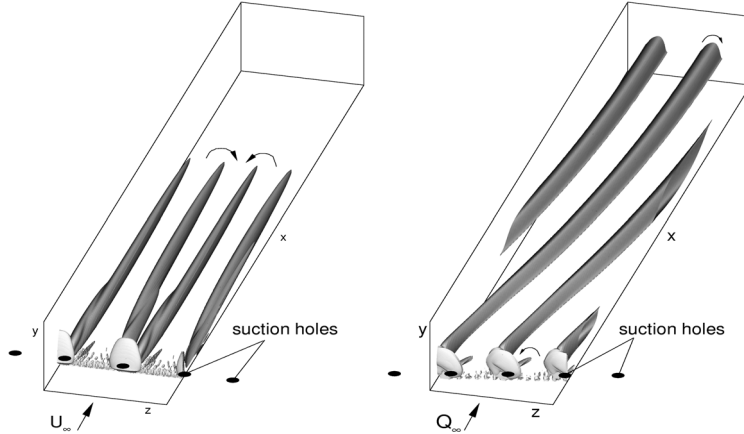


Fig. 2. Visualisation of vortices emanating from a single suction hole row on an unswept (left) and swept wedge (right). Coordinates x , y and z denote streamwise, wall-normal and spanwise direction, respectively. Arrows indicate the sense of vortex rotation. The direction of the basic crossflow points to the left (relevant in right figure only). Results are from DNS.

$$\frac{\partial \boldsymbol{\omega}}{\partial t} - (\boldsymbol{\omega} \cdot \nabla) \mathbf{u} + (\mathbf{u} \cdot \nabla) \boldsymbol{\omega} = \frac{1}{Re} \nabla^2 \boldsymbol{\omega} \quad (1)$$

$$\mathbf{u} = (u, v, w), \boldsymbol{\omega} = (\omega_x, \omega_y, \omega_z). \quad (2)$$

The solution is obtained in two substeps. First, a 3-d steady baseflow (denoted by the index B) is calculated which satisfies the assumption of an infinite swept wedge, i.e. a swept plate with well-defined streamwise pressure gradient ($w_B \neq 0$, $\partial f_B / \partial z \equiv 0$). In a second step the development of disturbances (denoted by a prime) generated by suction orifices, e.g. slits, slots, or holes, is simulated within the integration domain. All variables are normalised by the freestream velocity $\bar{U}_\infty = 159 \text{ m/s}$ and a reference length $\bar{L} = 9.434 \text{ mm}$. Simulations are carried out in a rectangular body-fixed integration box on the swept plate (Fig. 3). For calculations of the steady baseflow a velocity distribution $U_{Be}(x)$ is imposed at the freestream boundary $y = y_e$ according to a Falkner-Skan-Cooke (FSC)-type flow, $U_{Be} = U_0 x^m$, $m = \beta_H / (2 - \beta_H)$, $\beta_H = 0.5$, Hartree Parameter. A FSC-type boundary layer covers all essential properties of a 3-d flow in the front region of a wing at the lowest number of parameters. Suction is modeled by prescribing the wall-normal velocity at the wall:

$$v'(r) = -v_c \cos^3 \left(\pi \frac{r}{d} \right). \quad (3)$$

The ratio r/d results from the shape of the orifice. For spanwise slots with slot width d_{sL} (extension in x) and slot length L_{sL} (extension in z) follows, see Fig. 4:

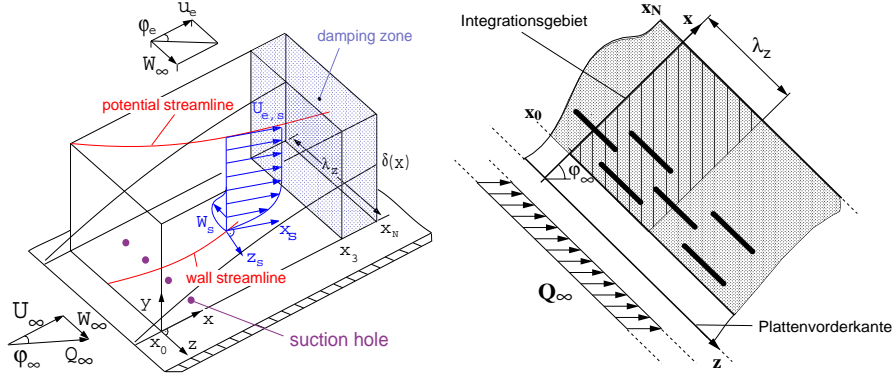


Fig. 3. Left: Perspective view on the integration domain with one spanwise row of suction holes. Right: Top view of swept plate with rows of spanwise slots.

For $z_{SL} \leq z \leq z_{SL} + L_{SL}$

$$d = d_{SL} \quad , \quad r = \sqrt{(x - x_{SL})^2} \quad , \quad r \leq \frac{d_{SL}}{2}$$

For $z < z_{SL}$

$$d = d_{SL} \quad , \quad r = \sqrt{(x - x_{SL})^2 + (z - z_{SL})^2} \quad , \quad r \leq \frac{d_{SL}}{2}$$

For $z > z_{SL} + L_{SL}$

$$d = d_{SL} \quad , \quad r = \sqrt{(x - x_{SL})^2 + (z - (z_{SL} + L_{SL}))^2} \quad , \quad r \leq \frac{d_{SL}}{2}$$

For suction holes with diameter d_L follows :

$$d = d_L \quad , \quad r = \sqrt{(x - x_L)^2 + (z - z_L)^2} \quad , \quad r \leq \frac{d_L}{2}.$$

In case of slots the suction velocity is constant over the slot length L_{SL} at each streamwise position. By imposing the \cos^3 -profile at the slot borders at $z = z_{SL}$ and $z = z_{SL} + L_{SL}$ a smooth crossover to vanishing suction velocities is ensured. Outside the slots or holes v' is zero at the wall. Exploiting the infinite-span condition, spanwise periodicity of the flow can be enforced:

$$f'(x, y, z, t) = f'(x, y, z + \lambda_z, t) \quad , \quad \left. \frac{\partial^n f'}{\partial z^n} \right|_{x, y, z, t} = \left. \frac{\partial^n f'}{\partial z^n} \right|_{x, y, z + \lambda_z, t} \quad . \quad (4)$$

Thus the disturbance-flow equations can be effectively discretised in spanwise direction by a fully complex Fourier spectral representation

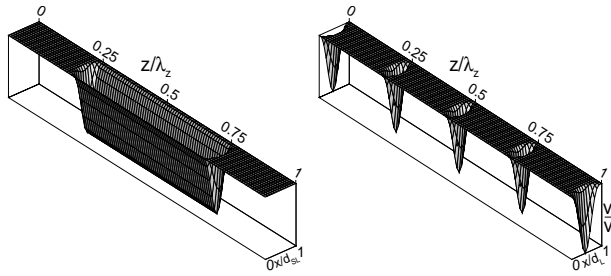


Fig. 4. Suction v' -velocity distributions in the spanwise-streamwise plane. Left: spanwise slot with $L_{SL} = 0.5\lambda_z$. Right: Holes with regular spacing $s_z = \lambda_z/4$ and diameter $d = s_z/5$. The streamwise direction x is stretched by a factor of 2.21.

$$f'(x, y, z, t) = \sum_{k=-K}^K F_k(x, y, t) e^{ik\gamma_0 z}, \quad F_{-k} = \text{conjug.}\{F_k\}, \quad (5)$$

where γ_0 denotes the fundamental spanwise wavenumber, related to the spanwise width λ_z of the computational domain through $\gamma_0 = 2\pi/\lambda_z$. The spatial derivatives in x - and y -direction are principally discretised with 6th-order compact Finite Differences. The step size in streamwise direction Δx is constant, and the wall-normal step size Δy can be halved up to three times in successive zones near the wall. The nonlinear terms of the vorticity transport equations are evaluated pseudospectrally using the 2/3-rule for de-aliasing. The discretised v' -Poisson equations are solved with a direct (Fourier) technique. Time integration is done with a fourth-order Runge-Kutta method. At the upper boundary, a wall-normal exponential decay of the v' -velocity is assumed except for mode $k = 0$, where a zero slope is enforced to match the results for asymptotic suction ($v(y) = v_0 = \text{const.}$). Upstream of the outflow boundary the well-proven enforced decay of the disturbance vorticity vector is employed to prevent undue disturbance reflections. More details of the numerical method are reported in [1, 9].

3 Computational Results

Due to the Fourier spectral representation eq. (5) the three-dimensional flow field splits in a set of $(K + 1)$ complex two-dimensional flow fields in Fourier space coupled by the nonlinear convective terms of the vorticity transport equation. Therefore parallel processing of the Fourier modes has been implemented in the numerical code except for the calculation of the nonlinear terms where in turn the streamwise direction is parallelised. The code has been executed on both nodes of the NEC SX-5 (each node having 16 processors and 32/48 GB RAM) of the hww GmbH, Stuttgart. On a single processor the code reaches 1,8 GFLOPS of 4 GFLOPS theoretical peak performance at a vector

operation ratio of 99% and an average vector length of 150. In multi-processor runs the code reached 93% of the optimal linear speed-up performance. The computation time was $1.5\mu\text{s}$ per time step and grid point on a computational grid $7201 \times 169 \times 37$. The maximum RAM requirement has been 24.4 GByte.

4 Results

4.1 Baseflow

An accelerated Falkner-Skan-Cooke boundary layer with Hartree-parameter $\beta_H = 0.5$ has been chosen as baseflow. The combination of sweep and chordwise pressure gradient leads to an inboard-oriented crossflow component -when viewing the wedge as an airliner wing- inside the boundary layer perpendicular to the mean flow direction. In the present baseflow the crossflow component $w_{s,B}$ continuously increases downstream and attains a maximum value of 13.5% at the outflow boundary. The flow is unstable with respect to stationary disturbances in a range of spanwise wavelengths from $433\mu\text{m}$ up to $3487\mu\text{m}$ at the inflow boundary $x_0 = 2.08$. Further downstream, the range of unstable wavelengths diminishes (Fig. 5).

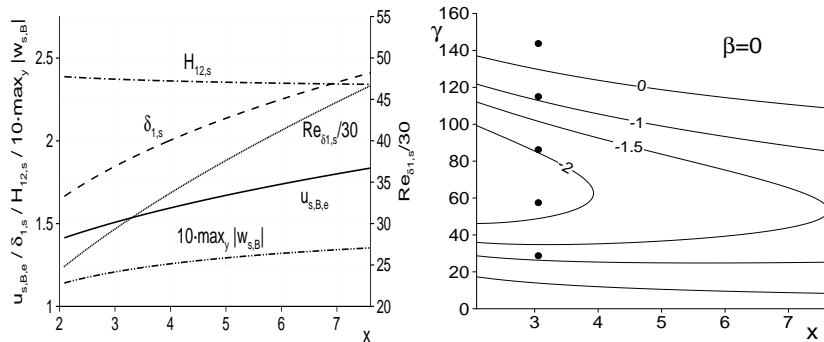


Fig. 5. Baseflow parameters (left) and contours of spatial amplification rates $\alpha_i = -\frac{1}{A} \frac{dA}{dx}$, A- disturbance amplitude, for zero frequency $\beta = 0$ according to linear stability theory (right). Dots indicate excited wavenumbers in the simulations presented in section 4.2.

4.2 Disturbance Excitation

A spanwise Fourier transform of the suction-velocity distribution reveals the excited disturbance spectrum. Two configurations as shown in Fig. 4 are discussed: a spanwise slot with a ratio of spanwise slot length to spanwise slot spacing $L_{sL}/s_z = 0.5$, and holes with a diameter $d_L = 1/20 \lambda_z$ and a spanwise

spacing $s_z = \lambda_z/4$. λ_z denotes the fundamental spanwise wavelength. Excitation of 3-d disturbances also depends on the porosity given by the ratio of open to closed surface. As for slot suction with naturally high porosity, only the wavenumber $\gamma_0 = 28.75$ corresponding to the spanwise slot spacing has a significant amplitude. For odd multiples the spectral amplitude decreases rapidly, the even multiples of the fundamental wavenumber γ_0 are excited as well since the slot velocity distribution possesses corner arcs at the lateral slot ends. A sharp cut-off of the suction distribution would result in zero amplitudes for even multiples of γ_0 .

Considering the row of holes having a lower porosity, the disturbance spectrum of excited spanwise wavelengths is much broader. In addition, the amplitude decay towards high wavenumber disturbances is smaller. Under the assumption of a homogeneous hole alignment with constant hole diameter d_L , constant spanwise hole spacing s_z , and constant volume flow per hole \dot{V} , only wavenumbers which correspond to s_z and their higher harmonics are excited. In such an idealised case, the amplitudes of all other disturbance modes are zero. Comparing the spectra shown in Fig. 6 one has to keep in mind that am-

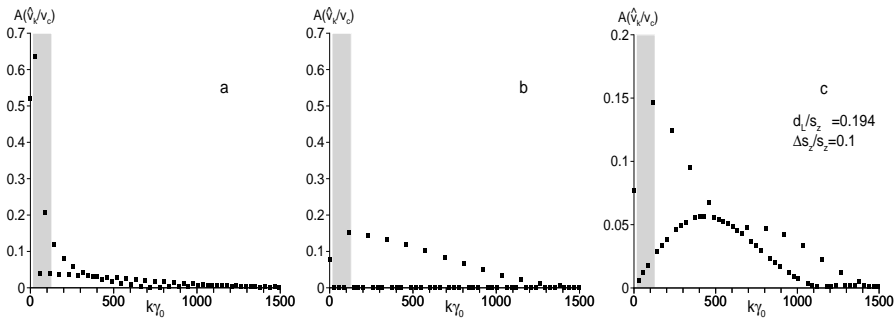


Fig. 6. Discrete amplitude spectrum of normalised wall-normal velocity distribution in the middle of the suction orifice. Left: spanwise slot, middle: hole row, right: hole row with spanwise offset of one hole. Shaded areas specify the unstable range according to linear stability theory at $x = 3.06$. Note the different ordinate scale in c.

plitude spectra of normalized velocities are plotted. The normalisation is done by the maximum suction velocity v_c . At a constant suction rate, decreasing porosity leads to an increase in maximum suction velocities. In our example v_c increases by a factor of 6.7 from the slot row to the hole row. Thus, for a comparison of effective suction velocities of the two spectra in Fig. 6a and 6b at equal suction rates, Fig. 6b has to be multiplied by 6.7. The grey zones in Fig. 6 correspond to the instability region according to linear stability theory at $x = 3.06$. Referring to the hole row the first amplitude peak is located within the instability region. This can be avoided through a narrower spanwise spacing of the holes, shifting the amplitude peak into the stable region.

Assuming an idealised regular spacing of identical holes it is therefore possible to completely avoid the excitation of primarily unstable disturbances. In this case, the spanwise spacing of the suction orifices has to be smaller than the smallest unstable wavelength.

However, in practice irregularities always occur either due to manufacturing imperfections and tolerances or due to clogging during operation. To illustrate the important aspect of inhomogeneities, one hole of the regular hole pattern shown in Fig. 4 is displaced by $d_L/2$ in spanwise direction. The spectral amplitude distribution reveals that now all wavenumbers are excited including the unstable ones, see Fig. 6c. This means that close spanwise spacing cannot prevent the generation of primarily unstable disturbances in any case.

4.3 Disturbance Development

The key point in a successful application of discrete suction is to minimise the generation of 3-d suction-induced disturbances. As pointed out in section 4.2 one way is to use slots, offering a relatively uniform suction distribution in spanwise direction. Slots only produce a significant excitation amplitude for the wavenumber corresponding to the spanwise slot spacing s_z for $L_{SL} \approx \frac{1}{2}s_z$. If this mode is damped or only weakly amplified no relevant additional generation of 3-d disturbances by the suction panel has to be expected and thus no 3-d effects can compromise the beneficial effect of the 2-d component $k = 0$ that represents the desired, primarily stabilising suction effect.

For verification a simulation of 35 equidistant slot rows was performed. A modal analysis in time of the flow field is performed to enable identification of any possible unsteadiness present. It reveals that a significant thus stabilising mean flow deformation represented by the mode (0,0) can be observed ($h\beta_0, k\gamma_0$; h, k denote multiples of fundamental frequency and fundamental spanwise wavenumber). Furthermore 3-d disturbances are indeed only moderately excited by slot suction (suction extends from $3 \leq x \leq 5$). Downstream of the slot array at $x = 7$ the 3-d disturbance amplitude is only slightly higher than in case of homogeneous suction. Homogeneous suction represents an ideally permeable wall and has been applied for comparison with equal suction rate. The primarily most unstable mode $\gamma = 57.5$ has been introduced upstream the suction panel for comparison, cf. Fig. 7. Disturbance excitation and amplification is still weak for hole arrays with a porosity as high as 3.7% and a spanwise hole spacing $s_z = 424\mu m$ which is smaller than the primarily unstable wavelengths. Although the excitation amplitude can be quite high at the beginning of the hole array damping downstream leads to negligible non-linear interactions between 3-d disturbances. Therefore no additional undesired disturbance generation is caused (Fig. 8).

Reducing the porosity at constant suction rate means increasing the suction velocities and the risk to exceed the valuable suction range. When exceeding critical values tripping of transition is observed, a phenomenon named *oversuction*. To study cases of oversuction a careful choice of the numerical step

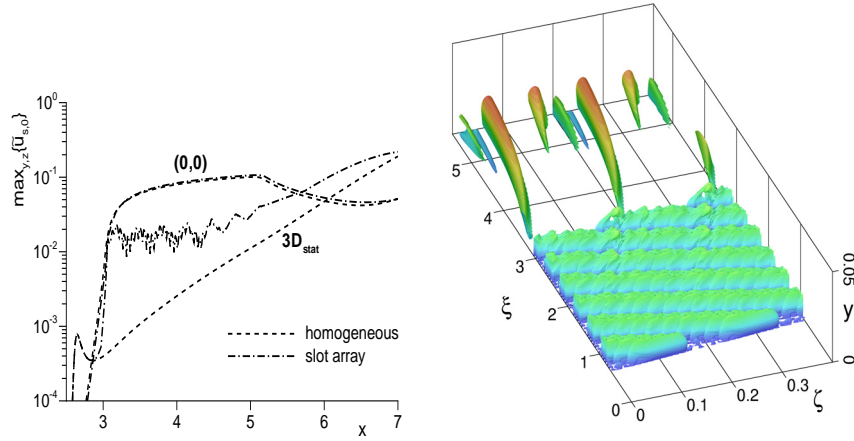


Fig. 7. t -modal amplitude development of stationary disturbances for suction through a slot array and homogeneous, ideal suction with an extra enforced steady mode from upstream for comparison (left). Vortex visualisation of slot-array suction (right). For sake of clarity the integration domain is rotated by 30° about the y -axis at $x = 2.5$. The distance from the wall is coloured from blue to red.

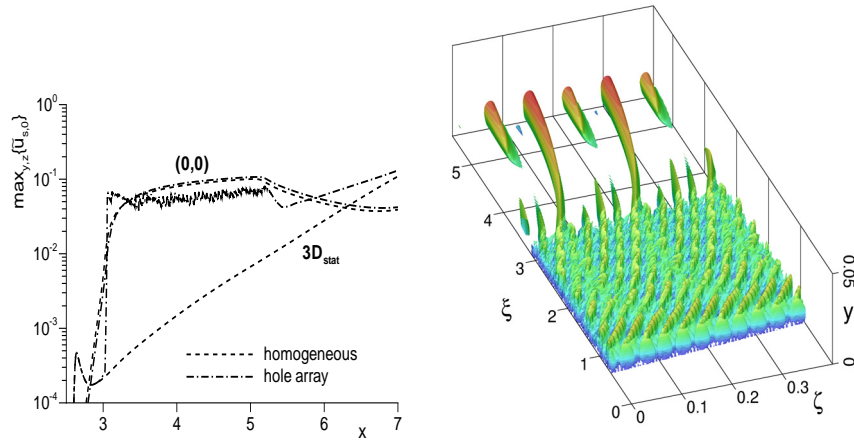


Fig. 8. As Fig. 7 but for a hole array with porosity $P = 0.037$.

sizes is mandatory to exclude any influence of the discretisation. Investigations for a single hole row in a 3-d boundary-layer flow revealed that insufficient numerical resolution can be the reason for a fast temporal growth of unsteady (numerical background) disturbances triggering the breakdown of laminar flow downstream of the hole row even in the absence of any time-dependent forcing. (This phenomenon indeed exists in 2-d baseflows and arises from a so-called absolute instability with timewise disturbance growth as present in bluff-body

wakes with strong reversed flow.) High suction velocities in combination with a spanwise hole spacing within the unstable range result in large 3-d disturbance amplitudes as well as in a wealth of immediate non-linear interactions between 3-d modes. Strong vortices emerge from the hole panel (Fig. 9, right). The mean flow is highly deformed and becomes susceptible to secondary instabilities. To determine whether a secondary instability occurs or not, a periodic pulse-like disturbance is enforced after saturation of the steady crossflow vortices. The t -modal analysis shows strong spatial growth of high-frequency disturbances downstream of the hole array (Fig. 9, left). This secondary instability is of purely convective nature as no timewise growth of unsteady disturbances is observed. Maximum secondary amplification rates appear at a frequency $\beta = 2\pi\bar{f}L/\bar{U}_\infty \approx 120$, $\bar{f} = 320kHz$, and are about four times larger than the maximum primary amplification rate of the most unstable unsteady crossflow mode at $\beta \approx 10$, $\bar{f} \approx 27kHz$. By means of flow visualisations in physical space finger-like vortices riding downstream on the primary vortices at their updraft side can be observed. Such finger vortices have already been identified in investigations of crossflow-induced transition where steady or traveling crossflow vortices trigger the transition process [8, 9].

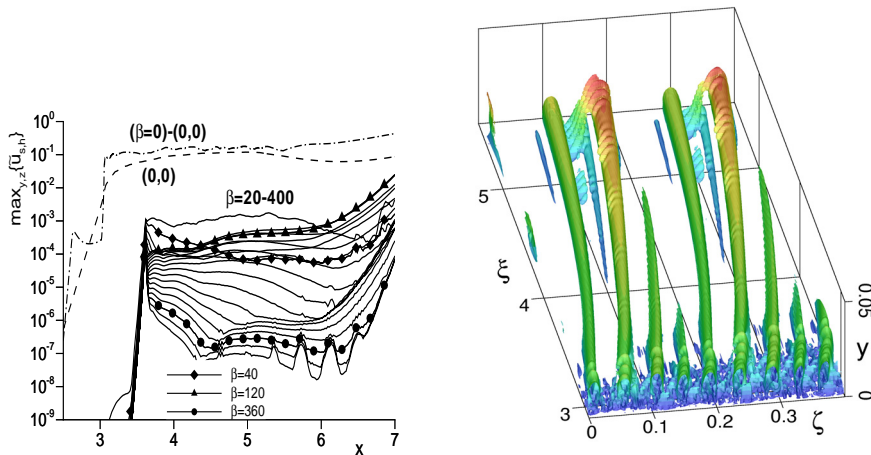


Fig. 9. t -modal amplitude development of stationary disturbances (left) and vortex visualisation (right) for a hole array with porosity $P = 0.024$ and periodic pulse-like forcing at $x = 3.7$.

5 Conclusions

In contrast to two-dimensional boundary-layer flows stationary disturbances can be primarily unstable in 3-d flows. Therefore special attention must be

paid to the excitation of steady 3-d disturbances through suction at the wall. By the varying wall-normal velocity at the wall along the span, undesired three-dimensional disturbances are generated. Thus, spanwise (continuous) slits are optimal. The stronger the non-uniformity of the suction distribution the higher are the amplitudes of possibly unstable crossflow (CF) modes. For spanwise slots or holes the spanwise spacing should be such that it is smaller than the smallest wavelength of amplified modes, or at least smaller than the most amplified wavelength. In case of a regular hole pattern this would guarantee that stable or only weakly unstable crossflow modes (and their higher harmonics) are generated. However, manufacturing imperfections and tolerances or clogging of holes always cause the excitation of a broad-band wavenumber spectrum including disturbances in the amplified range. Laminar flow control by suction can be successful as long as the suction-induced disturbances are small and non-linear interactions between the excited 3-d disturbances are negligible. In general, these conditions are not fulfilled for hole arrays unless the panel porosity is high and the spanwise hole spacing is small enough to lie in the range of again stable spanwise wavelengths, $s_z < 3\delta$, $\delta \equiv$ boundary-layer thickness (at the parameters considered $s_z < 600\mu m$). At high suction velocities premature transition is caused by a convective secondary instability primed by large-amplitude crossflow vortices. To prevent transition by oversuction the suggested procedure is to check the generated steady vortex patterns with respect to their potential to trigger secondary instability. We note that suction panels designed for the airliner, thus having a relatively low hole spacing s_z , can not be used for meaningful wind tunnel experiments if the windtunnel speed is lower than the flight speed. The s_z is just too low for the low speed case, leading to an unrealistically good result as for the excitation of disturbances. Recent work on slot arrays aims at an optimised slot order in spanwise/streamwise direction to avoid the excitation of unstable crossflow modes. A simply staggered order is useless due to the differing directions of the wall- and boundary-layer edge streamline, and the altered receptivity of the varying mean flow.

Acknowledgements

The financial support by DFG under grant Kl 890/3, as well as by Deutsche Airbus, grant No. 81947667, is gratefully acknowledged, as well as the provision of computer resources by HLRS within the project LAMTUR.

References

1. Bonfigli, G.; Kloker, M. : Spatial Navier-Stokes simulation of crossflow-induced transition in a 3-d boundary layer. In Nitsche, W.; Heinemann, H.-J.; Hilbig, R. (eds.), *New Results in Numerical and Experimental Fluid Dynamics II. Proc. 11. AG STAB/DGLR Symposium, NNF 72*. Vieweg Verlag, Braunschweig, 1999.

2. Bulgubure, C.; Arnal, D. : Dassault Falcon 50 Laminar flow flight demonstrator. In DGLR; AAf; RAeS (eds.), *Proc. First European Forum on Laminar Flow Technology, March 1992, Hamburg*. DGLR-Bericht 92-06, 1992.
3. Fowell, L. R.; Antonatos, P. P. : Some Results from the X-21 A Program - Part 2: Laminar Flow Flight Test Results on the X-21 A. In *Recent Developments in Boundary Layer Research*. Part IV, AGARDograph 97, 1965.
4. Maddalon, D. V. : Hybrid Laminar-Flow Control Flight Research. *Research and Technology, NASA, TM-4331*, p. 47, 1991.
5. Maddalon, D. V.; Collier, F. S.; Montoya, L. C.; Land, C. K. : Transition Flight Experiments on a Swept Wing with Suction. *AIAA-89-1893*, 1989.
6. Pfenninger, W. : Some Results from the X-21 A Program - Part 1: Flow Phenomena at the Leading Edge of Swept Wings. In *Recent Developments in Boundary Layer Research*. Part IV, AGARDograph 97, 1965.
7. Thibert, J. J.; Quast, A.; Robert, J. P. : The A320 Laminar Fin Programme. In DGLR; AAf; RAeS (eds.), *Proc. First European Forum on Laminar Flow Technology, March 1992, Hamburg*. DGLR-Bericht 92-06, 1992.
8. Wassermann, P. : *Direkte numerische Simulation zum querströmungsinduzierten laminar-turbulenten Umschlagprozess in einer dreidimensionalen Grenzschichtströmung*. Dissertation, Institut für Aerodynamik und Gasdynamik der Universität Stuttgart, 2002.
9. Wassermann, P.; Kloker, M. : Mechanisms and passive control of crossflow-vortex induced transition in a three-dimensional boundary layer. *J. Fluid Mech.*, **456**, 49–84, 2002.